Solar Energy 199 (2020) 782–795

Contents lists available at ScienceDirect

Solar Energy

journal homepage: www.elsevier.com/locate/solener

Design and analysis of dense array CPV receiver for square parabolic dish system with CPC array as secondary concentrator

S. Lokeswaran[a], Tapas K. Mallick[b], K.S. Reddy[a,*]

[a] Heat Transfer and Thermal Power Lab., Department of Mechanical Engineering, Indian Institute of Technology Madras, Chennai 600 036, India
[b] Environment and Sustainability Institute, University of Exeter, Cornwall, TR10 9FE, UK

ARTICLE INFO

Keywords:
Solar energy
Parabolic dish
Concentrating photovoltaic module
Optical ray tracing
CPC with homogenizer

ABSTRACT

In this paper, a two-stage square parabolic concentrating photovoltaic (CPV) receiver dish with an overall geometric concentration ratio of 500 suns is designed to provide a uniform intensity distribution on high-efficiency triple-junction solar CPV cell module. The system comprises of a square parabolic dish with an aperture area of 9 m^2 as a primary concentrator and an array of the compound parabolic concentrator integrated optical homogenizer of 0.27 × 0.27 m^2 as a secondary concentrator in tandem with the dish. The CPV module consists of an array of 12 × 12 triple junction CPV cells with each cell connected in parallel or series combination and integrated CPC homogenizer dedicated to each cell. The homogenizer length is selected based on the peak to average ratio of concentrated flux with the aim to maximize the optical and electrical performance of the CPV system. Monte Carlo ray-tracing model is used to predict the flux distribution. The predicted solar flux distribution on individual CPV cells are used as input to determine the electrical performances of the CPV module with three different cell interconnections. For optimized homogenizer length of 0.005 m and receiver height of 3.7 m, the maximum optical and CPV module efficiencies are obtained as 68.30% and 32.03% respectively. A year-round electrical power output of developed CPV system is 2.19 MWh which is up to 33.54% higher as compared to conventional CPV system. The proposed novel geometric design could accommodate the bypass diode for each cell, effectively reducing the current mismatch effects.

1. Introduction

Solar Photovoltaics (PV) is one of the most attractive direct electric energy conversion technologies available. The effective way to reduce the solar PV limitations like high cost semiconductor and its narrow band gap limit is to make use of concentrating photovoltaic (CPV). The Concentrating Photovoltaic (CPV) systems use optical devices like mirror to enable large area light collection on a smaller solar cell receiver area. The use of Multi-Junction (MJ) cells in a CPV system increases the power output due to its higher electrical conversion efficiency in the presence of concentrated solar flux. However, the complex tandem structure of MJ cell makes it relatively expensive when compared to conventional cells (Stolte, 1992). A potential way of reducing the cell cost is to operate it on sufficiently higher Concentration Ratio (CR). Increasing CR makes the system complex and expensive due to the need for more accurate tracking, increased pumping power for cell cooling due to high solar flux. To overcome these demerits, the electricity generated by CPV system must outweigh the additional parasitic power losses. Careful selection of the type of concentrator optics that directs the solar rays on CPV cells along with the effective cooling mechanism can exploit the promising potentials of the MJ cells thereby resulting in desired economic gain.

The required CR can be obtained by different reflection (mirror) or refraction (lens) type concentrators (Kumar and Rosen, 2011). The refractive Fresnel lens and mini dish concentrator are widely used primary concentrators in standalone applications due to their simple construction and operational flexibility (Xu et al., 2016; Wang et al., 2017). Although these approaches enhanced the flux uniformity to a certain extent, being single cell system there is serious limitation in achieving a CPV system with large power scale. To overcome this limitation, an array of single cells with point focusing concentrator is combined to form the large scale CPV system (Shanks et al., 2016). These discrete single cell point focusing systems has main disadvantage that the heat from the solar cells is dissipated passively to ambient air. As an approach to reduce the electricity generation costs, this surplus heat energy can be recovered by arranging the CPV cells in a matrix to form dense array receiver. The large area dense array CPV receiver with efficient active cooling technologies can convert solar energy into both

* Corresponding author.
E-mail address: ksreddy@iitm.ac.in (K.S. Reddy).

https://doi.org/10.1016/j.solener.2020.02.075
Received 22 August 2017; Received in revised form 1 January 2020; Accepted 21 February 2020

Nomenclature

A_C	Cell area (m^2)
$A_{CPC\ –\ in}$	Aperture area of CPC inlet (m^2)
$A_{CPC\ -\ out}$	Aperture area of CPC inlet (m^2)
A_{dish}	Aperture area of the dish (m^2)
$A_{receiver}$	Aperture area of the receiver (m^2)
$CR_{g\ CPC}$	Geometric CR of CPC (suns)
$CR_{g\ dish}$	Geometric CR of the dish (suns)
$CR_{g\ 2\ stage}$	Geometric CR of two-stage concentrator (suns)
D	Diameter of the dish (m)
E_{avg}	Average irradiation on the cell (W/m^2)
E_i	Instantaneous irradiation (W/m^2)
E_{ic}	Instantaneous irradiation on the cell (W/m^2)
E_{max}	Local maximum flux (W/m^2)
E_{min}	Local minimum flux (W/m^2)
F	Focal length of the dish (m)
I	Current (A)
I_{DNI}	Direct normal Irradiation (W/m^2)
I_0	Diode saturation Current (A)
I_{ph}	Photo current (A)
θ_a	Acceptance angle (degree)
L_{hom}	Length of homogenizer (mm)
M	Avalanche breakdown exponent
N	Diode ideality factor
P	Power (W)
$P_{E\text{-}h}$	Hourly averaged electrical power (W)
$P_{E\text{-}hd}$	Hourly average electrical power output (W)
$P_{E\text{-}hy}$	Annual average electrical power output (W)
P_{MP}	Maximum power (W)
R_s	Series resistance (Ω)
R_{sh}	Shunt resistance (Ω)
V	Voltage (V)
V_{br}	Diode break down voltage (V)
V_T	Thermal voltage (V)
η_C	CPV efficiency (%)
η_E	Electrical efficiency (%)
η_O	Optical efficiency (%)
θ_i	Incidence angle (degree)
ρ_{CPC}	Reflectivity of CPC (%)
ρ_{dish}	Reflectivity of the dish (%)
Σ	Total optical error (mrad)
σ_{slope}	Slope Error (mrad)
$\sigma_{specular}$	Specular reflectance Error (mrad)
σ_{sun}	Sun shape error (mrad)
σ_{track}	Tracking error (mrad)
Ψ	Rim angle of the dish (degree)

Abbreviations

1S-CPV	Single Stage CPV system
2S-CPV	Two Stage CPV system
A	Constant in diode equation
ACR	Average Concentration Ratio
CPC	Compound Parabolic Concentrator
CR	Concentration Ratio (suns)
CPV/T	Concentrating Photovoltaic / Thermal
CPV	Concentrating Photovoltaic
FHCR	Flux Heterogeneity of CR
FSS	Four String Series
NC	Cell Number
PAR	Peak to Average Ratio
PF	Packing Factor
SSS	Single String Series
TSS	Two String Series

Subscripts

y	Yearly average
m	Maximum
d	Days in a month

electricity and heat increasing the cogeneration efficiency of the system. It may be noted that the same primary concentrator i.e. refraction lens used for single cell CPV system cannot be applicable for dense array CPV system. Instead, a heavy and thick lens is required to obtain high CR, which may result in additional optical losses like coma and chromatic aberrations. Ancona et al. (2017) demonstrated successfully to overcome this limitation by using a parabolic dish concentrator which utilizes a reflective mirror. The parabolic dish concentrator uses reflective parabolic mirrors with large aperture area to concentrate the sunlight on the receiver with smaller area.

Another major challenge in dish CPV system is to achieve an acceptable homogenous and uniform irradiance distribution on CPV cell (Reis et al., 2015). Rim angle (ψ) is a widely used design parameter to distribute the solar irradiation flux as per the requirement. For instance, Jafrancesco et al. (2014) reported that the flux non-uniformity is more significant at larger rim angles (~52°). The reason being attributed to the curvature of the dish which produces Gaussian flux. According to Gunther and Shahbazfar (2011), the parabolic dish with lower rim angle ($\psi < 45°$) produces more uniform flux distribution than the higher ones ($\psi > 45°$) but the spillage loss is inevitable. In the literature, three major strategies have been adopted to overcome the spillage losses and improve the flux uniformity: (i) mounting homogenizer made of square reflective walls at the focus before the receiver (Kreske, 2002; Meller and Kribus, 2013), (ii) placing an transparent dielectric optical mixer in front of the receiver (Feuermann and Gordon, 2001), (iii) by using secondary optics (Victoria et al., 2009; Meller and Kribus, 2013; Bunthof et al., 2017), and (iv) maintaining a rim angle as low as 10° (Tan et al., 2014). These strategies have been implemented to minimize the cell to cell mismatch losses in a CPV receiver.

Besides the flux uniformity requirement for the CPV system, achieving high CR at the compact receiver by using the less cost large aperture reflective optics is also challenging. To maintain the required CR, Lovegrove et al. (2009) devised a robust mirror structure for single stage dish concentrator. However, higher CR necessitates larger dish aperture area for the same receiver area, which poses severe manufacturing and operating difficulties including increased tracking power due to high wind resistance. On the other hand, a Two Stage CPV (2S-CPV) concentrator alleviates the CR with improved uniformity and offsets the associated limitations of Single Stage CPV (1S-CPV) system. Taking advantage of the 2S-CPV, Lokeswaran et al. (2015) introduced a novel 2S-CPV system consisting of reflective CPC (made of mirror) concentrator integrated homogenizer for each cell to concentrate and homogenize the solar radiation on the cell array. The preliminary findings show that the homogenizer tends to reduce the local cell non-uniformity and thereby preventing the unwanted lateral currents in the cell. Yew et al. (2015) and Chong et al. (2017) used secondary refractive CPC array made of a dielectric material. It may be noted that, the dielectric secondary concentrator works based on refraction principles and incur optical losses like Fresnel losses from the interface (between cell and CPC) reflection (Otanicar et al., 2015), material absorption (Luque and Hedgedus, 2006) and chromatic aberration due to wavelength dependent refractive index (Kurtz, 1996). Also, the chromatic aberration under wide solar spectrum will increase due to high CR and aging. In contrast, the mirror CPC works on reflection principle

and overcomes most of the demerits, except the reflection losses in the optical path.

From the foregoing literature review, it is apparent that 1S-CPV systems have lower efficiency because of the inherent optical and electrical mismatch losses. Several alternates have been reported to overcome the demerits of 1S-CPV system; there is a scarcity of work reported on the usage of 2S-CPV system. Thus, in the present work, a comprehensive attempt is made to design a new 2S-CPV system with relatively more efficient reflective secondary concentrator in tandem with a primary square parabolic dish concentrator. Towards this, Monte-Carlo ray tracing simulations are proposed to optimize the length of the homogenizer as well as to investigate the ensuing performance improvements. Finally, the optical and electrical performance parameters of the designed 2S-CPV system are analyzed and further benchmarked with the conventionally available 1S-CPV dense array receivers.

2. Design and description of the proposed CPV system

The new CPV design has been carried out as a part of the Bio-CPV project (Mallick et al., 2013) with an objective to develop and integrate highly efficient solar, biomass and hydrogen energy technologies. The schematic of the proposed square parabolic dish with receiver, electrical and thermal load is shown in Fig. 1. The CPV system consists of primary parabolic dish concentrator which focuses sunlight to the CPV receiver mounted at the focus. The specifications of the same are provided in Table 1. The CPV receiver is made of the secondary concentrator mounted in line with the CPV cell assembly. The secondary concentrator is made of an array of CPC integrated homogenizer that accepts the reflected rays from the dish. The redirected and concentrated solar flux falls on the CPV cell assembly mounted at homogenizer exit aperture for efficient energy conversion. The CPV cells convert a significant portion of the solar energy to electricity. The unconverted spectrum of solar flux heats up the cells that are subsequently dissipated by an active cooling system. The electrical and heat energy generated by the system is connected to electrical and thermal loads, respectively. The efficiency of the cell increases with the logarithm of the concentrated flux intensity and reaches the highest value of current density at 500 suns (Azur Space, 2014). The system is designed to attain an overall geometric CR of 500 suns, because further increasing concentration decreases the cell efficiency due to the ohmic losses (Nishioka, 2006). The overall geometric CR of a 2S-CPV system is the product of the geometric CR of both the primary and secondary concentrators, and is given as:

$$CR_{g2stage} = CR_{gdish} \times CR_{gCPC} \tag{1}$$

The geometric CR of the dish is defined as the area ratio of the square parabolic dish to CPV receiver and is estimated as follows:

$$CR_{gDish} = \frac{A_{dish}}{A_{receiver}} \tag{2}$$

The geometric CR of CPC based on the acceptance angle of the CPC (θ_a) and aperture size is calculated using the expression:

$$CR_{gCPC} = \frac{1}{\mathrm{Sin}^2\,\theta_a} = \frac{A_{CPC-\,in}}{A_{CPC\,-out}} \tag{3}$$

In a 2S-CPV system, the acceptance angle of the CPC (θ_a) should be greater than or equal to the rim angle to accept all the radiation from the parabolic dish concentrator (Joseph, 2008). The dish with very low rim angle results in increasing spillage loss because of the reflected rays

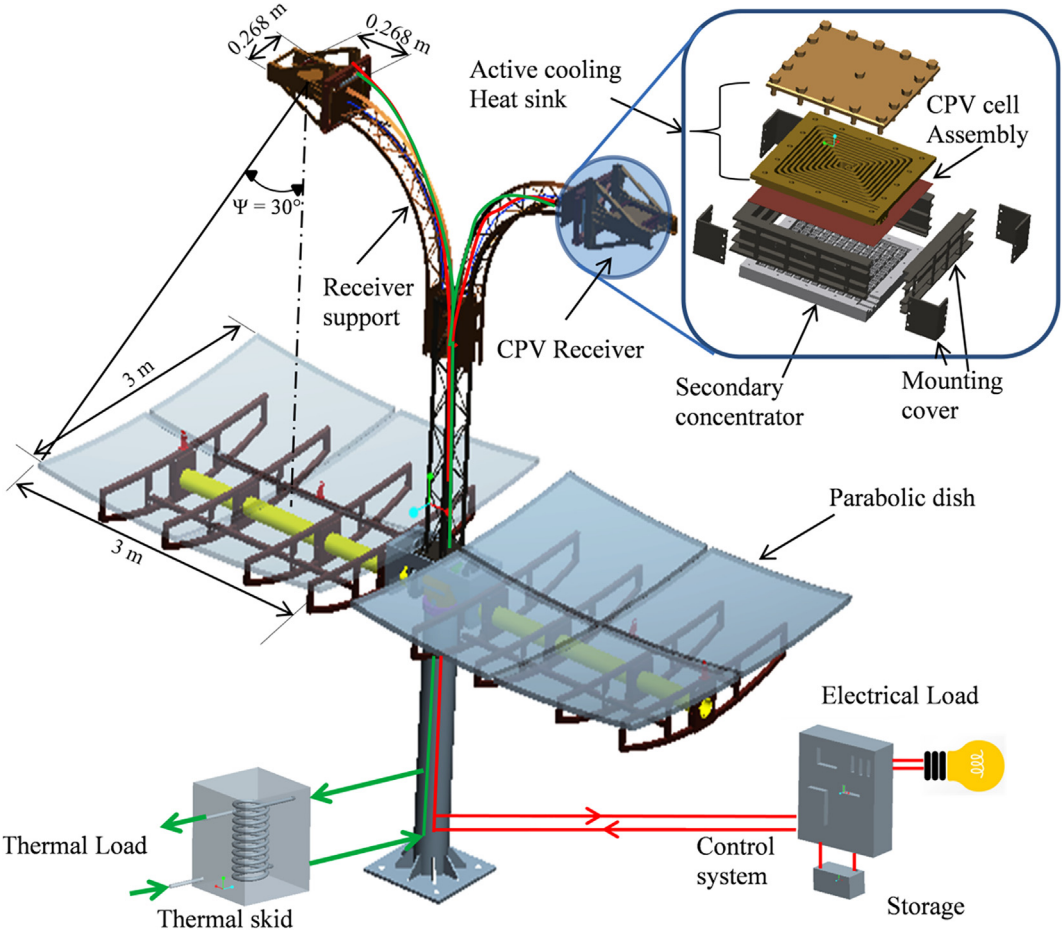

Fig. 1. The schematic of square parabolic dish with CPV receiver, electrical and thermal load connected.

Table 1
Geometrical and Optical parameters of solar parabolic dish with CPC concentrator.

Parameter (dish)	Value	Parameter (CPC)	Value
Concentration ratio (CR_{dish})	125	Concentration ratio (CR_{CPC})	4
Aperture area (A_{dish})	3 × 3 m^2	Entry aperture area ($A_{CPC\text{-}in}$)	0.02 × 0.02 m^2
Focal length (f)	3.7 m	Exit aperture area ($A_{CPC\text{-}out}$)	0.01 × 0.01 m^2
Rim angle (ψ)	30°	Half Acceptance angle ($\theta_a/2$)	30°
Reflectivity (ρ_{dish})	94%	Homogenizer dimensions (l × l)	0.01 × 0.01 m^2
		Reflectivity (ρ_{CPC})	90%

hitting outside the receiver aperture. On the other hand, a larger dish rim angle significantly reduces the CR of CPC as evident from Eq. (3). Therefore, in this study rim angle (ψ) of 30° is selected as the best compromise resulting in minimum reflections on CPC with reasonable $CR_{g\ CPC}$ of 4 suns (Rabl, 1976). Furthermore, the selected rim angle results in better trade-off between the peak flux and uniformity of flux distribution when compared to theoretically maximum flux produced at rim angle of 45°. Assuming the exit aperture of the CPC equal to the CPV cell size, for selected $CR_{g\ CPC}$ the Eq. (3) is used to estimate the dimension of the entry aperture of CPC as 0.02 m × 0.02 m. The secondary concentrator is then formed by an array of 12 × 12 CPCs arranged in a series of row and column. The area of the secondary concentrator is 0.268 m × 0.268 m with an inevitable manufacturing tolerance of 0.0005 m between the CPCs and 0.0115 m mounting space each side. Based on the calculated receiver area ($A_{receiver}$) and selected geometric CR of the dish ($CR_{g\ dish}$), the area of the parabolic dish (A_{dish}) is calculated by Eq. (2). The area fraction of receiver ($A_{receiver}$) to effective dish aperture ($A_{dish} - A_{receiver}$) is lower than 0.8% and thus the shadow of the receiver on dish aperture can be neglected.

2.1. Design of primary concentrator

The square parabolic dish reflector of 3 m × 3 m aperture area and $\psi = 30°$ with geometric CR of 125 suns is used as the primary concentrator to focus the solar radiation on receiver focal plane. The relation between the focal length to diameter (f/d) ratio and rim angle of the dish is given as (Stine and Harrigan, 1985):

$$\frac{f}{d} = \frac{1}{4\tan(\psi/2)} \tag{4}$$

For a selected rim angle and diameter, the focal length of the dish is calculated by Eq. (4) is found to be 3.7 m. The mirrors are made of 0.005 m thick solar grade glass with the back-coated reflective surface of 94% reflectivity (Meyen et al., 2009). The dish is tracked using 2-axis slew gear mechanical tracking system.

2.2. Design of secondary concentrator with homogenizer

The secondary concentrator is made of an array of 12 × 12 three dimensional symmetric CPCs integrated homogenizer arranged side by side to accommodate the 144 cells and the schematic is shown in Fig. 2. It is located at the receiver height (shifted or adjusted focal length) of the dish to collect as many reflecting rays from the dish and uniformly illuminate on the entrance area of the square CPV cell array. The dimensions of secondary concentrator without mounting tolerance are 0.02455 m × 0.02455 m (sum of 12 $A_{CPC\text{-}out}$ with 0.0005 m manufacturing tolerance in-between the CPCs). Further, the Packing Factor (PF) is the ratio of active receiver cell area illuminated to the total receiver area facing concentrated solar flux and it is found to be 0.95 for the 2S-CPV receiver. The three dimensional CPC is made up of two different parabolas whose axes are inclined at an acceptance angles ± θ_a (30°) to form total angle of 60°. The solar ray with angle of incidence (θ_i) ranging between the acceptance angle $-\theta_a \le \theta_i \le \theta_a$ is received into the CPC and reflected towards its exit aperture. The entry aperture of homogenizer is mounted at the exit aperture of CPC with the common optical axis. The CPC has square shape entry and exit aperture with dimensions of 0.02 m × 0.02 m and 0.01 m × 0.01 m (to match CPV cell), respectively. The CPC produces non-uniform flux distribution at the exit aperture with CR of 4 suns. The hollow reflective homogenizer with entrance and exit apertures of 0.01 m × 0.01 m collects the non-uniform rays reflected by the CPC, homogenizes by multiple reflections and redirects the same to the CPV cell.

2.3. CPV cell assembly

The CPV cell with dimensions of 0.01 × 0.01 m is connected in parallel to 0.005 × 0.01 m bypass diode and this sub assembly is mounted on the top thin copper layer of Insulating Metal Substrate

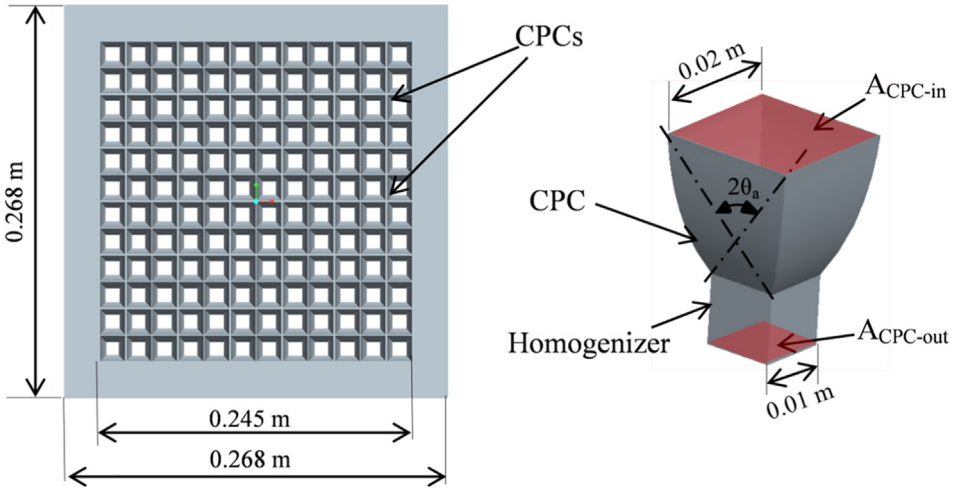

Fig. 2. Secondary concentrator.

(IMS). Several subassemblies are arranged to form an array of 12 × 12 on IMS as proposed by Micheli et al. (2015) is shown in Fig. 3. Depending on the cell interconnections, the power output of the array is extracted out from the 144 cells through external contacts. The space between the cells facilitates the series or parallel or combined cell electrical interconnection.

3. Investigation of the performance of dish with CPC

To estimate the distribution of the concentrated radiant flux on the CPV cell, optical ray tracing is adopted. Details on optical modeling strategies such as optical model description, associated errors, ray stability study, model validation are discussed extensively in subsequent sections. Besides, the output from the optical model is used as input for validated electrical model of the CPV array.

3.1. Optical performance modeling of CPV system

The optical model of the CPV system under investigation is presented in Fig. 4. It consists of a parabolic dish at center of global coordinates (X = 0, Y = 0, Z = 0), secondary concentrator and a ray source plane. Leveraging the advantage of axis-symmetric nature of the geometry, the analysis is conducted for the array of 6 × 6 cells (positive quadrant) which is one-fourth of complete 12 × 12 cell array and the results are then extended to entire array. The cell surface (target plane) is divided into a two-dimensional grid where the cells are represented by Cell Number (NC), for example, NC = 11 that denotes the cell in 1st row and 1st column and NC = 12 denotes the cell in 1st row and 2nd column. The results are discussed in terms of cells located along the diagonal (NC = 11 to 66) which are sufficient to represent the data for complete 12 × 12 array of cells. The receiver height is adjusted to achieve minimum average CR of 100 suns on the CPV cell located at the corner NC = 11. The ACR for cells are calculated based on 550 W/m^2 the annual average DNI for Chennai, India (Kumar et al., 2013).

3.1.1. Optical methodology

The Advanced Systems Analysis Program (ASAP® 2014V1 SP1) from Breault Research Organization (BRO) is used to evaluate the optical performance of the CPV receiver. Harvey isotropic scattering model is used with a threshold intensity of 1×10^{-12} for child ray below which it will cut off. Fig. 5 describes the algorithm of ray tracing. Histories of optical interaction of each ray from source plane to cell surface are sequentially traced and the results are exported and processed using MATLAB 2014. The sun shape error 3.6 mrad (milli radian) (Rabl, 1985), reflector surface slope error as 2 mrad for dish with f/d of 0.6 (Grossman et al., 1991), specular reflection as 0.3 mrad (Meyen et al., 2009) and tracking error assumed to be 1.5 mrad (Helwa et al., 2000) are used. The total optical error of a concentrator is the sum of the errors considered in the analysis (Jaffe, 1982).

The optical efficiency (η_O) is defined as the ratio of energy reaching at the receiver to the solar energy input to the parabolic dish aperture (Duffi and Beckman, 2013) and is given as:

$$\eta_o = \frac{\sum_{i=1}^{i=144} E_i A_C}{I_{DNI} A_{dish}} \tag{5}$$

The Flux Heterogeneity of CR (FHCR) is a measure of the relative percent of greatest non-uniformity on the CPV cell. It is defined as the ratio of the difference between local maximum flux and local minimum flux to the local average flux (Kreske, 2002) and is estimated as:

$$FHCR = \frac{E_{\max} - E_{\min}}{E_{avg}}\left(\frac{100}{2}\right) \tag{6}$$

The Average Concentration Ratio (ACR) on the cell is defined as the ratio between the sum of local incident flux to the area of the cell and is given as:

$$ACR = \frac{{}_{AC}\int E_{i\,c}\, dA_c}{A_{cell}} \tag{7}$$

The Multi-junction (MJ) solar cells performance under non-uniform illumination experiences a drop in open-circuit voltage, Fill Factor (FF) and efficiency when compared to a cell under uniform illumination (Herrero et al., 2010). The Peak to Average (PAR) ratio is a measure of local non-uniformity and defined as the ratio of local maximum flux to the local average flux on the cell and is evaluated as follows:

$$PAR\ ratio = \frac{E_{\max}}{E_{avg}} \tag{8}$$

3.1.2. Ray stability study

In optical ray tracing, the ray stability solution is essential to eliminate the effect of number of rays. Therefore, the variation of optical efficiency with respect to the number of rays is analyzed and the results of the same are shown in Fig. 6. It is noticed that, for increasing number of rays from 30 to 30000, the optical efficiency varies with number of rays and oscillates from 47.73% to 73.10%. With further increase in the number of rays to 3,000,000, the optical efficiency tends to decrease and ultimately stabilizes at around 68.3%. Hence, the solution is considered to be independent for three million numbers of rays as any further refinement produces almost constant optical efficiency with a maximum variation of 1%.

3.1.3. Validation of optical model

Validity of the simulation model is assessed by comparing the

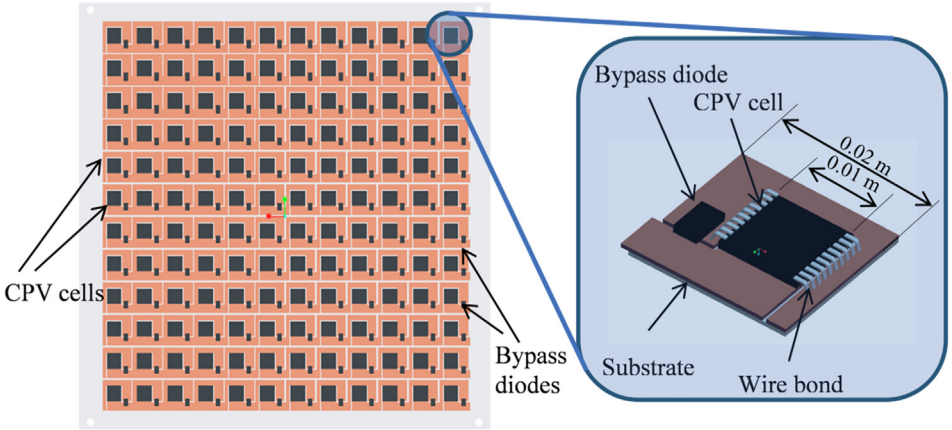

Fig. 3. CPV cell assembly with Insulating Metal Substrate (IMS) and cell interconnections.

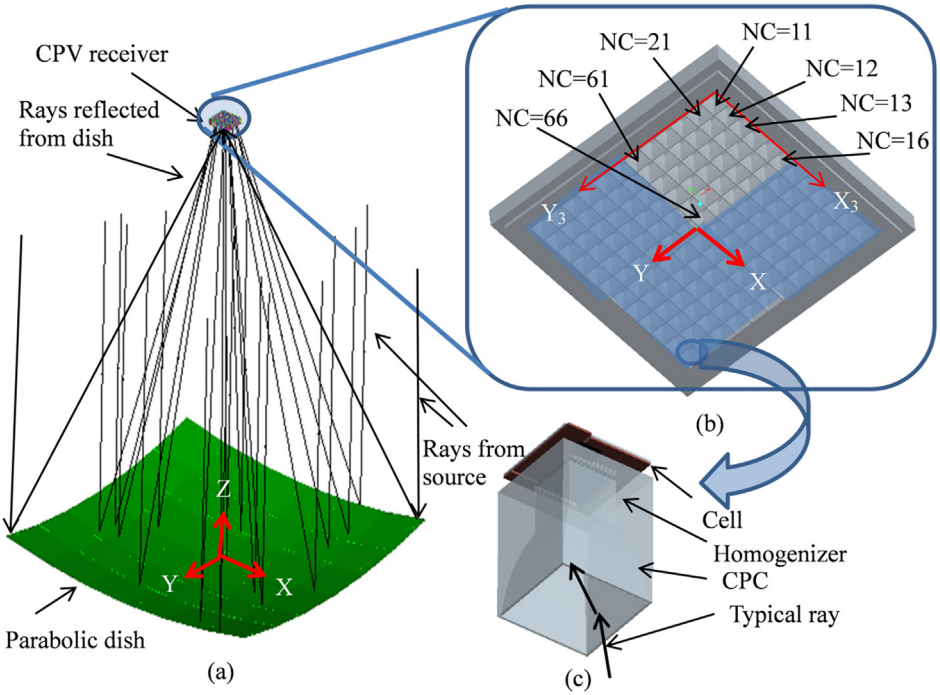

Fig. 4. Optical model and ray tracing of CPV dish (a) Square parabolic dish with receiver (b) The 6 × 6 CPC integrated homogenizer array with cell numbers (NC) (c) Isometric view of a CPC integrated homogenizer with a CPV cell and bypass diode.

predicted concentrated flux of the parabolic dish with the data available in literature (Johnston et al., 2003) and the same is presented in Fig. 7(a). The simulation is repeated for the same dish with different surface slope errors of 0, 2, 3 and 4 mrad and is presented. It is found that the predictions obtained using ray tracing technique are matching reasonably well with the data reported in literature. The deviation is 2 to 14% for slope error of 0 and 5 mrad, respectively, which is well within the acceptable limit.

3.2. Electrical performance modeling of CPV module

The power output of the proposed CPV system depends on the

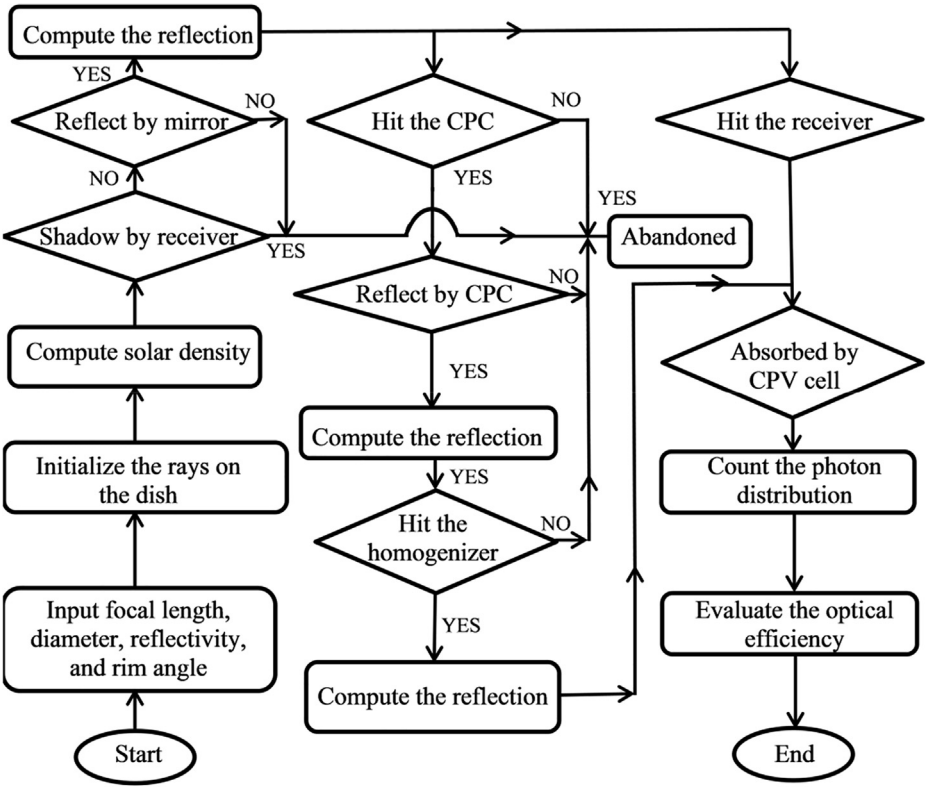

Fig. 5. Flowchart of optical ray tracing used in the simulation.

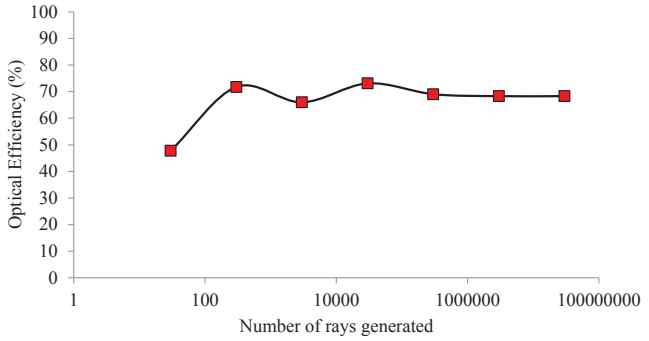

Fig. 6. Effect of number of rays on the optical efficiency of the CPV system.

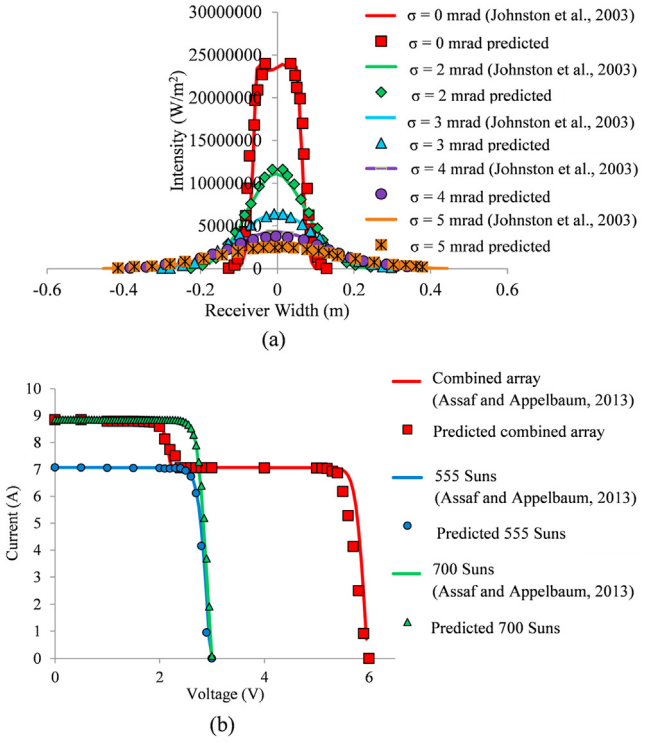

Fig. 7. Validation of the present study (a) Solar flux distribution with Johnston et al. (2003) on the flat receiver (b) Current-Voltage I-V curve characteristics with Assaf and Appelbaum (2013).

incident ACR and temperature of the CPV cell. The copper loss due to joule heating is negligible as discussed by Micheli et al. (2015). Though the equivalent electrical circuit of the cells can be modeled as single and double diode model, one-diode equivalent circuit model (Segev et al., 2012) is adequate and the same is implemented in this study. The I–V characteristic model equation with bypass diode and diode avalanche breakdown is used (Assaf and Appelbaum, 2013). The electrical output is calculated in terms of I-V curve using MATLAB code with extracted cell parameters. The commercially available 3C44 CPV cell with a thickness of $190 \pm 20 \times 10^{-6}$ m is used in present work (Azur Space, 2014). Since the active heat sink is used to dissipate the heat from the cell, the temperature of the cell is assumed to be constant at 25 °C.

The cell equivalent parameters required to solve the solar cell model equations are estimated by Newton Raphson method reported by Asaf and Joseph (2013). The parameters are estimated for four different light concentrations: 100, 250, 500 and 1000 suns at a cell temperature of 25 °C. The predicted maximum power is compared with the manufacturer data and found to be in good agreement. The maximum percentage deviation is 0.02, 0.09, 0.02 and 0.04% for CR of 100, 250, 500 and 1000, respectively. The estimated equivalent parameters for different concentrations are given in Table 2 and are interpolated for other CR. Further, the input flux conditions for the simulation of I–V and P–V curves of the receiver is taken from the optical ray tracing.

The CPV module efficiency (η_C) is defined as the ratio of electrical power produced to the power available at the CPV receiver of the CPV module (Siaw et al., 2014). It accounts for electrical series resistance and mismatch loss and is given as:

$$\eta_C = \frac{P_{MP}}{PF\,\eta_{optical}\,I_{DNI}A_{dish}} \tag{9}$$

The electrical efficiency (η_E) of the CPV system is a measure of overall electrical performance and is defined as the ratio of electrical power produced to the power input to the CPV system (Yew et al., 2015) and the expression to evaluate the same is as follows:

$$\eta_E = \frac{P_{MP}}{I_{DNI}A_{dish}} \tag{10}$$

The hourly average electrical power generated is calculated by hourly averaged DNI using the I-V and P-V curves obtained using:

$$P_{E-h} = I_m\,V_m \tag{11}$$

The annual average electrical power output is evaluated by the cumulative daily average electrical power over the month as given below:

$$P_{E-y} = \sum_{Jan}^{Dec}\sum_{d=1}^{d=30}\sum_{t_1=07:00\,hrs}^{t_2=18:00hrs}\frac{P_{E-h}}{t_2 - t_1} \tag{12}$$

3.2.1. Validation of electrical model

The solar cell equivalent model is solved with the estimated cell parameters and the predicted results are then compared with the data reported by Assaf and Appelbaum, (2013) to examine the validity of the model. Fig. 7(b) presents the comparison of current- voltage characteristics obtained using the present model and the data reported in literature for different ACR and cell combinations. Thus, the I-V curves corresponding to the single cell and two cells (connected in series) for ACR of 555 and 700 suns are plotted by running several simulations. It is noticed that the predicted results deviated by 2.10, 2.30 and 11.60% for cell with ACR of 555, 700 and combined array, respectively. The predicted results are compared with the data from literature and are found to be in good agreement.

4. Results and discussion

The results of this study are divided into three sections. In first section, the optimization of the length of homogenizer in terms of PAR to achieve better optical performance is considered. Subsequently, the

Table 2
Estimated parameters for CPV cells (Azur Space, 2014) under different concentrations.

Concentration Ratio (Suns)	I_{ph} (A)	Ln (I_0 (A))	n	R_s (Ω)	R_{sh} (Ω)	α	V_{br} (V)	m
100	1.54	−89.10	1.25	5.50×10^{-2}	450	6.28×10^{-5}	−0.6	14
250	3.85	−85.88	1.30	3.00×10^{-2}	400	5.13×10^{-5}	−0.6	11
500	7.66	−80.11	1.40	1.70×10^{-2}	330	7.32×10^{-5}	−0.6	9
1000	15.35	−68.07	1.63	1.61×10^{-3}	300	6.13×10^{-5}	−0.6	6

electrical output of the proposed CPV system is predicted in terms of I-V curve from the predicted flux distribution and is compared with conventional receiver. Finally, the annual energy output of the proposed and conventional CPV receiver is evaluated and compared.

4.1. Optical performance analysis of CPC integrated homogenizer

Influence of homogenizer on the flux distribution on the array of cells mounted on the CPV module is investigated by considering the flux distribution on unit cell (NC = 66) in the array. Ray of light from the source plane enters the aperture of CPC integrated homogenizer and subsequently falls on the cell surface which is mounted on homogenizer exit aperture as shown in Fig. 8. Though the geometric CR of designed CPC is 4 suns, the CPC without homogenizer will produce local non-uniform flux distribution on the cell near the corners and edges as evident from Fig. 8(a). It is due to the reflected flux from CPC surface that can reach more than 25 times of the incident rays at the inlet aperture of the CPC. Further, the homogenizer fixed at the exit aperture of the CPC will redistribute the peak flux distribution on the periphery of the cell surface towards cell center through multiple reflections. The redistribution of the flux by increased homogenizer length of 0.004 m results in the relocation of the peak flux from all four corners towards the center of the cell as shown in Fig. 8(b). Although the non-uniformity could not be completely eliminated, the flux profile is quite uniform at a particular homogenizer length due to trade-off between the reflection loss and flux uniformity. If the length of homogenizer increases further to 0.01 m, the peak flux merges and moves towards the cell center resulting in a Gaussian flux profile. This further enhances the flux non-uniformity with more reflection loss as apparent from Fig. 8(c).

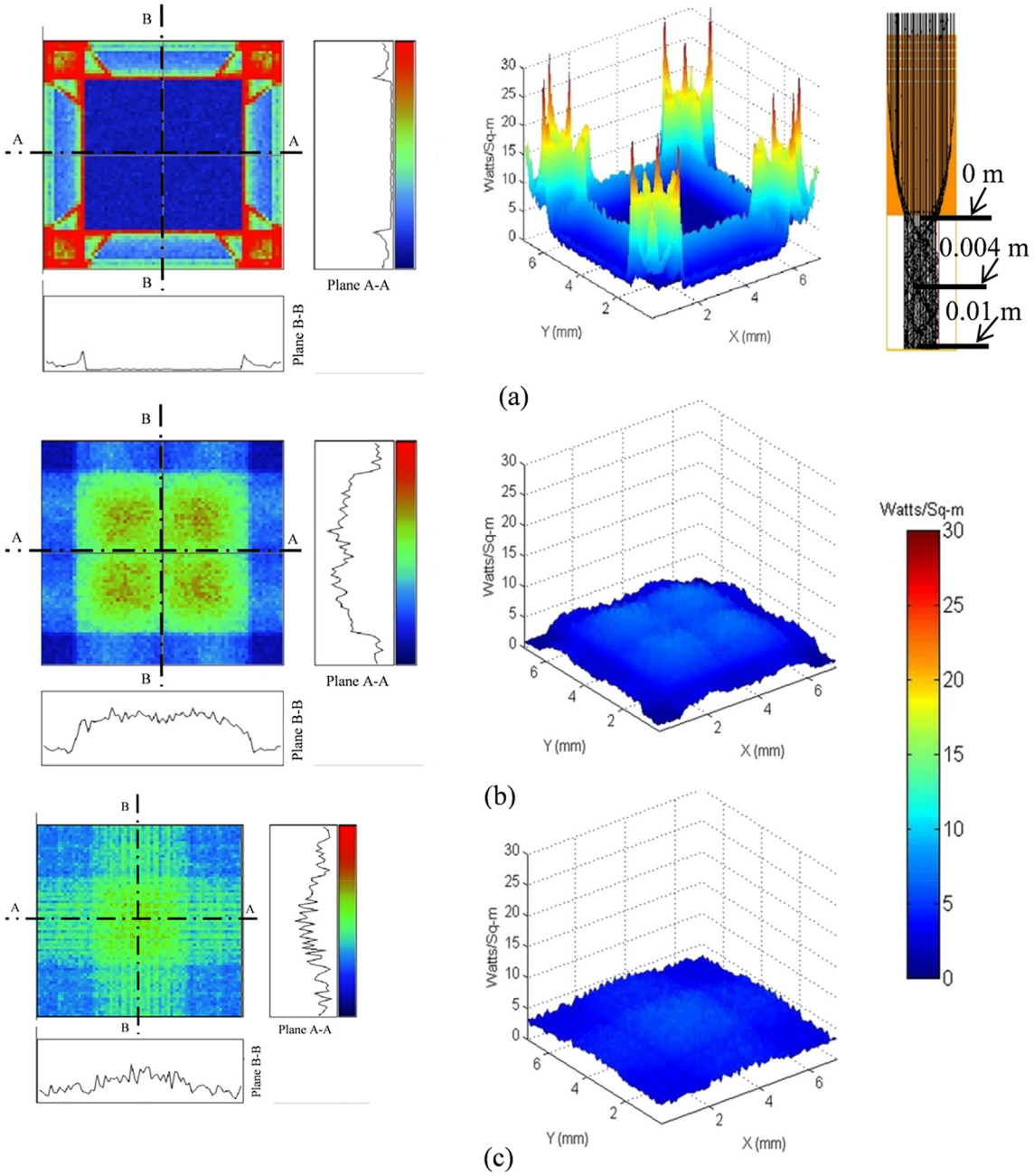

Fig. 8. Effect of homogenizer length on the CPV cell flux distribution of an ideal single CPC integrated homogenizer for (a) L_{hom} = 0 m, (b) L_{hom} = 0.005 m (c) L_{hom} = 0.01 m.

4.1.1. Effect of homogenizer length on flux heterogeneity of CR

As a measure of flux non-uniformity, the Flux Heterogeneity of CR is calculated using Eq. (6) for different homogenizer lengths (L_{hom}) varying from 0 to 0.025 m. Influences on Flux Heterogeneity of CR (FHCR) with respect to the homogenizer length for the cells located at the diagonal from corner to the center of CPC array (N_C = 11–66), is shown in Fig. 9. As the length of the homogenizer increases from 0 to 0.01 m, the cells in the array exhibit the common behavior of drastic oscillatory decrease forming the first local minima. With further increase in L_{hom}, the oscillating downward trend decays, forming the third or fourth minima and subsequently flattened out due to reflection loss. The cell that lies close to dish center axis (NC = 66) reaches local minima in relatively shorter L_{hom} of 0.005 m, whereas comparatively longer L_{hom} is required for cell located far away (NC = 11) due to low energy flux. Since the first local minima occurs within L_{hom} of 0.005 m for the cells, NC = 22–66 located close to dish axis, L_{hom} = 0.005 m is considered as optimized homogenizer length. Beyond this L_{hom}, further increase in homogenizer length may marginally improve the uniformity at the expense of additional reflection losses. This results in low power output and hence overall economic gain is questionable. The FHCR for L_{hom} = 0 m and L_{hom} = 0.005 m on the cells NC = 11 to NC = 66 are shown in Table. 3.

4.1.2. ACR and PAR ratio distribution over the 6 × 6 cell array

The influence of homogenizer length on Average of Concentration Ratio (ACR) and PAR ratio on the cells located at receiver diagonal NC = 11–66 is shown in Fig. 10. The ACR is calculated using Eq. (7) wherein the maximum radiation without homogenizer is 553 suns on the cell NC = 66 which gradually reduces to 202 suns at the corner cell NC = 11. The predicted minimum, maximum and ACR for all the cells are then utilized to calculate the PAR using the Eq. (8). The PAR of cells NC = 11–66 varies in the range of 3.22–2.51 and 2.50–1.51 for L_{hom} = 0 and 0.005 m, respectively. Also, flux non-uniformity of parabolic dish resulted in local variation of ACR over the cell array NC = 11, 44 and 66 as shown in Fig. 11(a)–(c). It is observed that due to high non-uniformity of the flux, the PAR of the cell NC = 66 is 2.6 when L_{hom} = 0, and reduces to 1.5 for L_{hom} = 0.005 m. on the other hand, further increase in L_{hom} to 0.010 m, the PAR reduced to 1.2 which is an insignificant improvement considering the fact of increase in reflection losses. The optical efficiency reduces from 74.59 to 68.30% for increase in L_{hom} from 0 to 5 mm. Further increasing the L_{hom} to 10, 15, 20 and 25 mm reduces the optical efficiency to 62.75, 58.05, 54.05 and 50.59%, respectively. The PAR of proposed CPC integrated homogenizer is lower and more uniform when compared to the PAR reported by Yew et al. (2015).

4.2. Comparison of 2S-CPV with 1S-CPV receiver

The proposed 2S-CPV receiver design is compared with existing 1S-CPV design configuration to appreciate its performance benefits. The receiver for 1S-CPV is conventional dense array consisting of the 12 × 12 CPV cells soldered on the IMS substrate. This six-cell series connected in parallel with a bypass diode forms a subassembly and similar sub-assemblies (Raed et al., 2002) are connected together in series to form the entire CPV receiver cell assembly as shown in Fig. 12. Due to the lack of the space to accommodate the diode for each cell inside this array, it is located at the side of the dense cell array. The bypass diode and associated cell interconnections between the cells in 1S- CPV receiver results in lower packing factor of 0.81 when compared to the PF (0.95) of 2S-CPV receiver. Also, the ineffective utilization of receiver space area that is directly illuminated does not contribute to power generation. Further, the CPV receiver length for 1S-CPV is calculated by the sum of the length of total number of cells (cell size of 0.010 m × 12) and cell interconnection length. The electrical cell interconnection length includes the fabrication tolerance of 0.0015 m and front metal contact of 0.00025 m on each side of the CPV cell. The 1S-CPV receiver area is relatively smaller having overall dimensions of 0.163 m × 0.163 m with mounting space length of 0.015 m each side. From Eq. (2), the aperture area of dish for 1S-CPV is determined as 3.2 m × 3.2 m. Moreover, the parabolic dish has the same rim angle as 2S-CPV dish, except it is designed to obtain a geometrical CR of 500 suns in a single stage. The 1S-CPV receiver height is adjusted to achieve minimum ACR of 100 suns on the corner CPV cell NC = 11 to avoid extremely small electrical power output due to the very low concentration near the edge of the receiver.

The flux distribution of the parabolic dish on the receiver plane of both 2S-CPV and 1S-CPV systems are shown in Fig. 13. For 1S-CPV system, the Gaussian non-uniform concentrated flux with peak flux of 852 from dish falls directly on the CPV receiver (CR g dish = 500 suns). When compared to 1S-CPV system, the concentrated flux of dish for 2S-CPV system is more uniform with peak flux of 226 suns (CR g dish = 125). Both the flux distributions are of square shape to accommodate the receiver area of 0.15 m × 0.15 m and 0.27 m × 0.27 m for 1S-CPV and 2S-CPV dish, respectively. Since the concentrated flux distribution of dish for 1S-CPV system is narrow than 2S-CPV system, the optical errors and variation of the receiver plane height have a severe effect on the optical efficiency due to spillage loss.

The difference in concentrated flux from the center axis of the dish to the edge on 11–16 and 11–66 CPV cells are presented in Fig. 14. For 2S-CPV, the ACR progressively increases from 175 suns to 277 suns and 175 suns to 556 suns for NC = 11–16 and NC = 11–66 respectively. The ACR for all the cells in the 2S-CPV system is more than the corresponding ACR in the 1S-CPV system except cells NC = 55, 56, 65 and 66. It is because the CPC aperture of 2S-CPV intercepts the incoming radiation which results in reduction of losses associated with the specular reflection, scattering and spillage as compared to 1S-CPV receiver. Larger dish aperture of 1S-CPV resulted in narrow peak flux, thus ACR of the cells NC = 55, 56, 65, 66 for 1S-CPV system are higher than the 2S-CPV system.

4.3. Electrical performance of CPV receiver

Three different cell interconnection designs have been developed and investigated with the aim to increase the electrical power output of the CPV cell assembly. The electrical power output of the CPV module depends on the cell interconnection and non-uniform flux distribution on cell array. A bypass diode is connected in parallel to the cell in the array or string to protect the cell from current mismatch due to the non-uniform flux distribution. Comparison of the electrical performance of 1S-CPV and 2S-CPV receivers in terms of cell interconnection layout, I-V and P-V characteristics and efficiency is presented subsequently.

4.3.1. Electrical cell interconnection layout

The Single String Series (SSS) cell interconnection layout is the simplest of all and is formed by connecting all the 144 CPV cells in an array of 12 × 12 cells in series. It results in open circuit voltage of

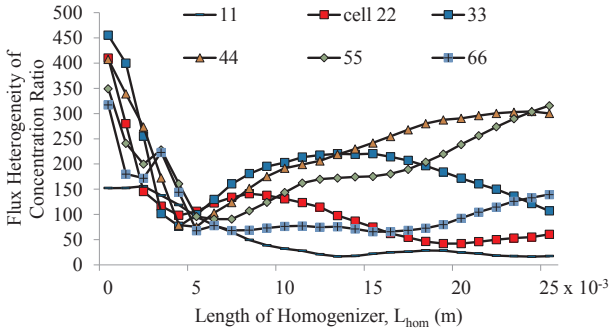

Fig. 9. Effect of homogenizer length on flux heterogeneity of concentration ratio on CPV cell for N_C = 11–66.

Table 3
FHCR and PAR for different NCs.

NC	FHCR		PAR	
	L_{hom} = 0 mm	L_{hom} = 5 mm	Predicted	From Yew et al. (2015)
11	152	95	2.42	2.35
22	410	106	1.6	2.16
33	455	99	1.37	2.09
44	407	75	1.29	2.11
55	349	111	1.39	–
66	317	172	1.51	–

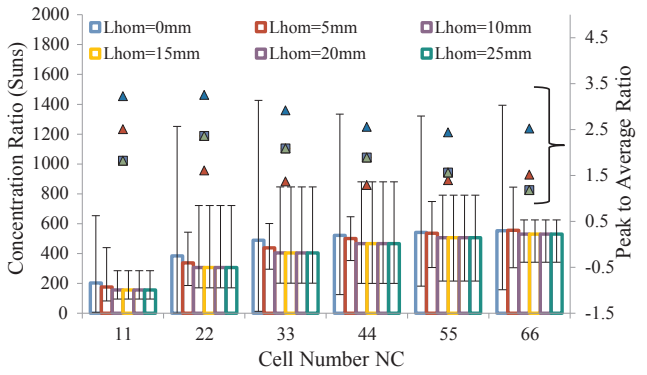

Fig. 10. Effect of homogenizer length on average concentration ratio and peak to average ratio over the CPV cells for N_C = 11–66.

447.84 V and short circuit current of 7.66 A. The Two String Series (TSS) cell interconnection is made by dividing the SSS cell interconnection layout into two separate strings of 72 series connected cells.

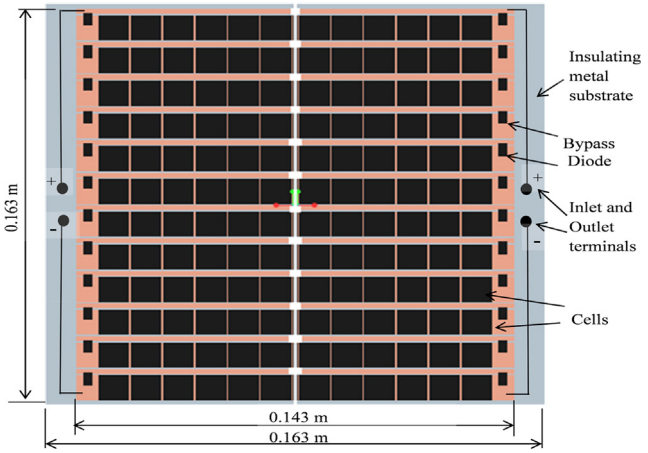

Fig. 12. The Single Stage CPV (1S-CPV) receiver design with CPV cells and bypass diode (Raed et al., 2002).

It consists of two series connected strings NC = 11–72 and NC = 73–144 both connected in parallel to increase the output current with open circuit voltage of 223.92 V and short circuit current of 15.32 A. Further division of the SSS electrical layout into four symmetrical series strings (S-I, S-II, S-III and S-IV) with 36 cells in each string leads to Four String Series (FSS). Alternately it is formed by splitting the TSS cell interconnection, resulting in a string that consists of 36 cells connected in series as shown in Fig. 15(a). The open circuit voltage and short circuit current of an individual string is 111.96 V and of 22.98 A. The electrical layout for 1S-CPV receiver configuration is similar to 2S-CPV with the exception that there are limited bypass diodes located on the sides of the cell array. The bypass diode is connected in parallel to a string of six series connected cells with SSS electrical layout as shown in

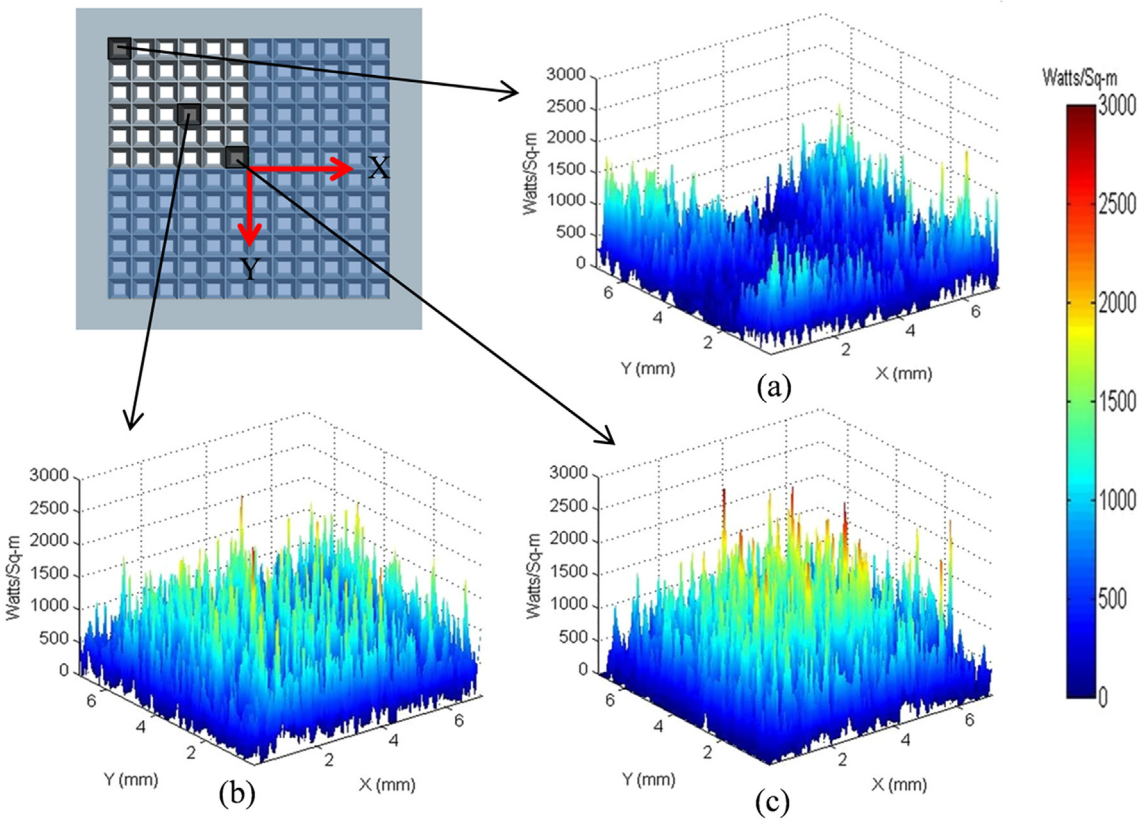

Fig. 11. The solar flux distribution over the CPV cells with homogenizer length L = 0.005 m for different cell numbers on the CPC array (a) NC = 11 (b) NC = 44 (c) NC = 66.

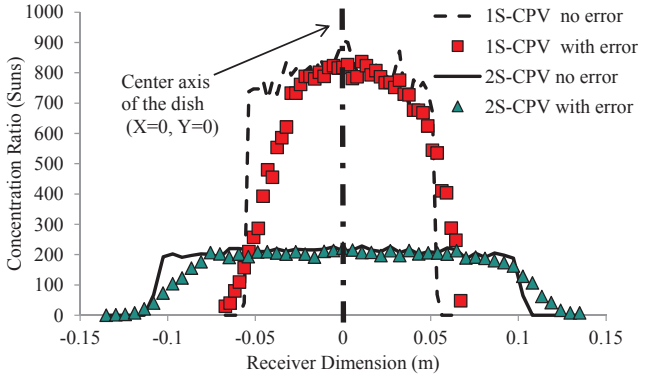

Fig. 13. Solar flux distribution from 1S-CPV and 2S-CPV dish on the entrance of the secondary receiver.

Fig. 15(b). For the other two electrical layouts namely TSS and FSS, the cell interconnection of 1S-CPV is similar to the 2S-CPV system.

4.3.2. I-V and P-V characteristics for 2S-CPV and 1S-CPV systems

The electrical performance of CPV systems in terms of I–V and P–V curves is simulated using the equivalent solar cell model. The predicted results for 2S-CPV and 1S-CPV systems are presented as shown in Fig. 16(a) and (b), respectively. The appearance of steps on both I-V and P-V curves indicate current mismatch on the cells in the array operating in the negative voltage range and forcing the bypass diodes to conduct. The maximum power of the module lies on the knee of the steps usually near the last steps of the I-V curve. The 2S-CPV system has maximum power output of 1.776 kW, 1.784 kW and 1.871 kW for SSS, TSS and FSS designs, respectively.

Less number of steps with a significant current drop on I-V curve of 1S-CPV receiver indicates the current mismatch between the different strings where six cells are connected to a bypass diode. The drastic drop in the maximum output power for the 1S-CPV system is because of the effect of high flux non-uniformity with low flux on the periphery cells in the array. The power outputs for 1S-CPV system with SSS, TSS and FSS designs are 0.706 kW, 0.719 kW and 0.836 kW, respectively. Thus, the 2S-CPV system results in more power output than the 1S-CPV system, as the presence of secondary concentrator with new CPV receiver reduces local cell non-uniformity and cell to cell mismatch losses.

4.3.3. Effect of cell interconnection on the power output of CPV system

The maximum electrical power output for 2S-CPV and 1S-CPV system with FSS cell interconnection is 1.871 and 0.836 kW, respectively. It is noticed that the power output of 2S-CPV receiver with FSS cell interconnection is 4.6% more than TSS which is 0.44% more than the basic SSS cell interconnection. For 1S-CPV receiver, the TSS and FSS cell interconnections improve the power output of SSS cell interconnection by 1.8% and 13.99%, respectively. Since, larger number of series interconnection segments (S-I to S-IV) connected in parallel tend to reduce the current mismatch losses, FSS cell interconnection has relatively higher power output.

4.3.4. Effect of cell interconnection on the efficiency of CPV system

The optical, CPV module and electrical conversion efficiencies of 1S-CPV and 2S-CPV system are shown in Fig. 17 as calculated by Eqs. (5), (9) and (10), respectively. Since usage of secondary receiver significantly reduced the spillage losses, the optical efficiency of the 2S-CPV system is found to be 68.30% which is quite higher than 59.72% for 1S-CPV system. Thus, even though there are additional reflection losses from CPC and homogenizers of 2S-CPV optics, the use of secondary concentrator enhances the optical efficiency and flux uniformity. Further, the CPV module efficiency determines how effectively the module works for a given irradiation irrespective of the optical losses. Since the individual cells in 2S-CPV receiver are equipped with by-pass diodes, the 2S-CPV receiver have a higher module efficiency of 30.41%, 30.54% and 32.03% for SSS, TSS and FSS configurations, respectively. The corresponding module efficiency for 1S-CPV are lower due to series resistance drop and are 15.78%, 16.05% and 18.67% for SSS, TSS and FSS configurations, respectively. Moreover, the electrical conversion efficiency of the 2S-CPV module for three string configurations namely SSS, TSS and FSS are 19.73%, 19.82% and 20.78% whereas, for 1S-CPV it is 6.90%, 7.02% and 8.16%. FSS and SSS cell interconnections have shown highest and lowest electrical conversion efficiency for both 2S-CPV and 1S-CPV receivers.

4.4. Annual performance of 1S-CPV and 2S-CPV systems

The electrical power for the proposed CPV system is evaluated by using actual weather data for different seasons in Chennai with the aim to compare the annual electrical performance. Since there is no official measured data for the hourly solar Direct Normal Irradiation (DNI) in Chennai (12.65°N, 79.74°E), Tamil Nadu, the data is taken from MNRE book (Ajit, 2009). The hourly average DNI profile for a particular day (15th day) of every month used for simulation of the CPV system is shown in Fig. 18. For the purpose of better representation, only the DNI data for March, June, September and December are given and it is advised to refer the source for remaining months.

The monthly and annual average electrical power output of both 1S-CPV and 2S-CPV systems with different interconnection configurations are calculated by Eq. (12). The year-round results of the electrical model for both 1S-CPV and 2S-CPV system for the given DNI are shown in Fig. 19. The 2S-CPV gives more monthly electrical power output than

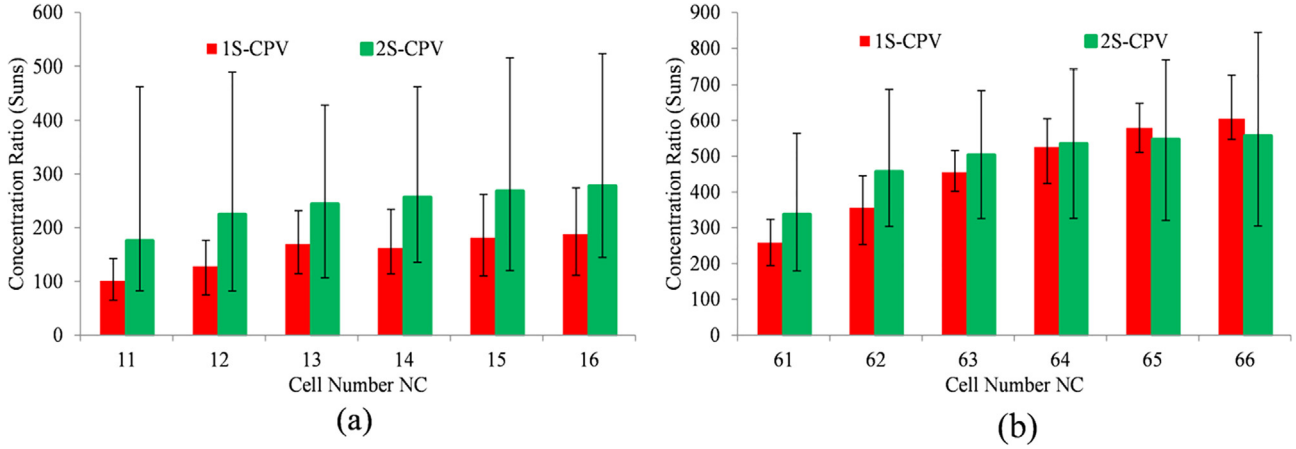

Fig. 14. Average Concentration ratio over the CPV cells with homogenizer length of 0.005 m for cell number (a) NC = 11–16, (b) NC = 11–66.

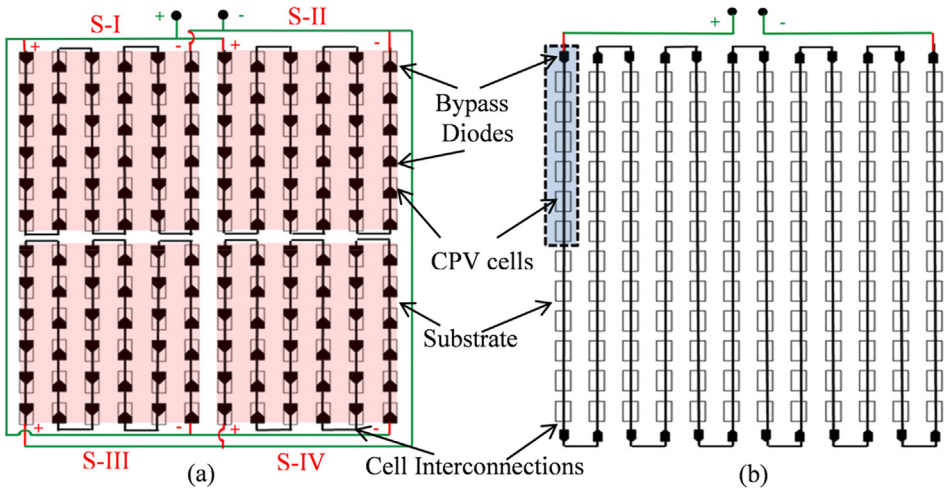

Fig. 15. Electrical layout of CPV cells with bypass diode in the CPV module (a) Four String Series (FSS) for 2S-CPV system (b) Single String Series (SSS) for 1S-CPV system.

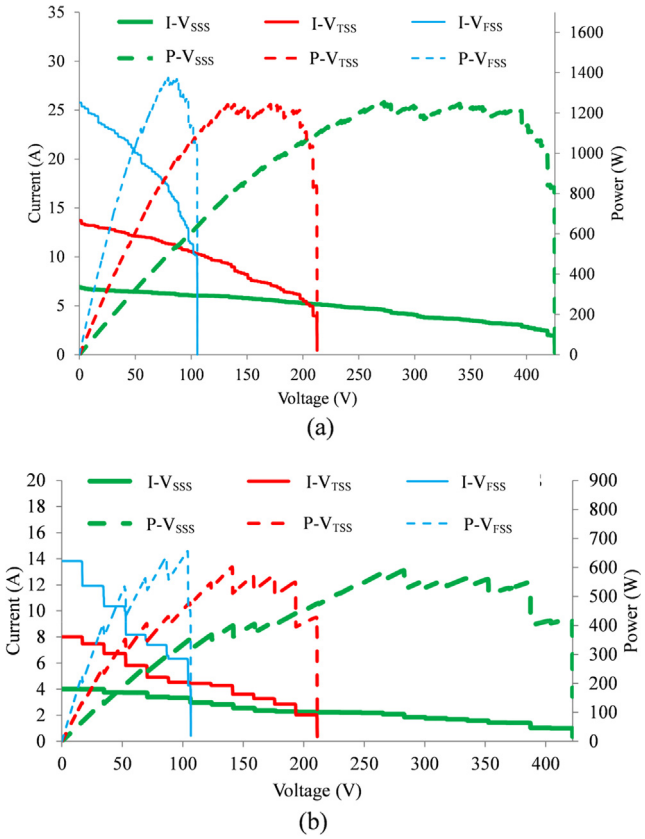

Fig. 16. I-V and P-V curves for SSS, TSS and FSS cell interconnections of the (a) 2S-CPV and (b) 1S-CPV receivers.

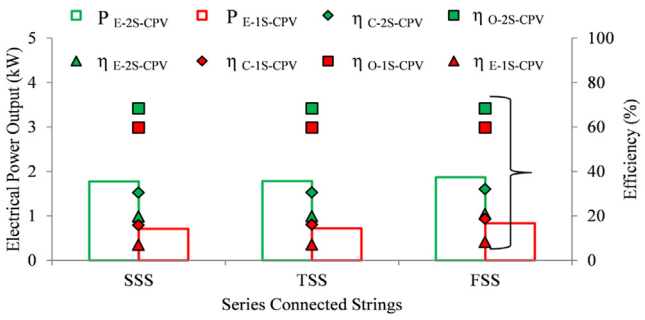

Fig. 17. Effect of string connections on the electrical power output, optical, CPV and electrical efficiency for 2S-CPV and 1S-CPV receivers.

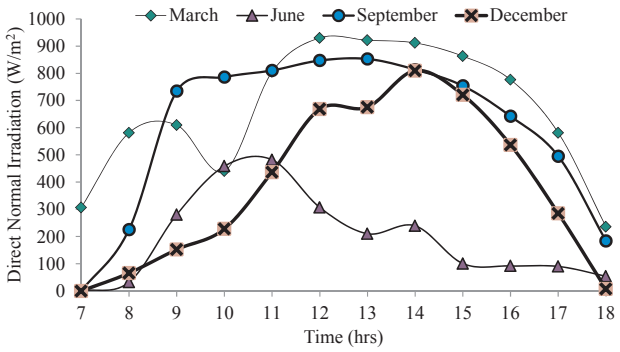

Fig. 18. Monthly Direct Normal Irradiation (DNI) used in simulation.

the 1S-CPV system due to the presence of individual bypass diode for each cell. With the maximum DNI of 930 W/m^2, the month of March has the maximum electrical output as 256.35 kWh for 2S-CPV and 150.07 kWh for 1S-CPV system. Likewise, for the month of September the maximum DNI is 852 W/m^2 and the corresponding electrical power outputs for 2S-CPV and 1S-CPV are 237.83 kWh and 140.12 kWh, respectively. On the other hand, the minimum power output is noted in the month of June as 137.90 kWh and 129.13 kWh for 2S-CPV and 1S-CPV system, respectively.

The maximum energy output for 2S-CPV system is 2.19 MWh and corresponds to FSS connection which is more than the other two configurations TSS (2.17 MWh) and SSS (2.12 MWh). On the other hand, the electrical power output for 1S-CPV configuration is 1.45 MWh, 1.62 MWh and 1.64 MWh for SSS, TSS and FSS configurations respectively. Thus, the power output of 1S-CPV is lower than 2S-CPV due to the current mismatch losses associated with the six-cell series connected to a diode. The FSS cell interconnection with 2S-CPV is preferred because of its higher power output.

5. Conclusions

A Comprehensive design of novel Two Stage concentrating photovoltaic (2S-CPV) system consisting of a square parabolic dish (primary concentrator) in tandem with an array of CPC integrated homogenizer (secondary concentrator) and CPV receiver is presented. The 2S-CPV receiver with three electrical interconnection layouts are introduced

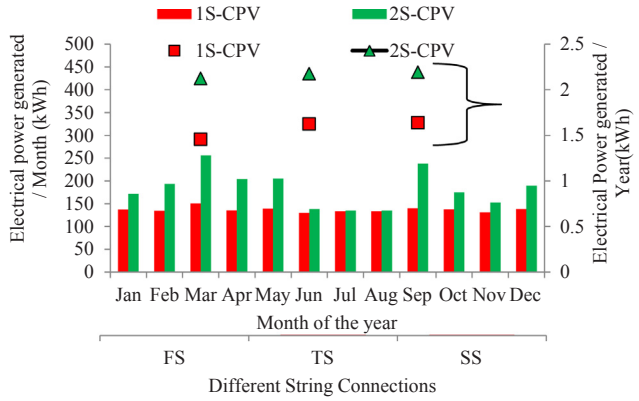

Fig. 19. Energy produced by both 1S-CPV and 2S-CPV system designs over one-year period.

and systematically analyzed towards better optical and electrical performance. The performance of present 2S-CPV system is compared against a conventional Single Stage (1S-CPV) system. Based on the extensive investigation the findings are listed as follows:

- The concentrated solar flux uniformity on the CPV cells in terms of peak to average Ratio is found to be in the range of 1.6 to 2.4. Based on the PAR, the optimized homogenizer length is arrived at 0.005 m.
- For the specified receiver height of 3.7 m, and optimized homogenizer length of 0.005 m, the maximum optical and CPV module efficiency of 2S-CPV receiver with FSS cell interconnection are found to be 68.30% and 32.03%, respectively.
- The year-round cumulative electrical power output from 2S-CPV estimates 2.19 MWh and thus showed an improved electrical performance up to 33.54% over the conventional 1S-CPV system.
- The drastic improvement of electrical performance with 2S-CPV system is due to the presence of integrated homogenizer, which improves local cell uniformity. Simultaneously, the CPC aids in reducing current mismatch losses due to the cell to cell non-uniformity by accommodating the bypass diode.

The overall enhanced performance of the proposed 2S-CPV system facilitates standby utility scale power generation, thereby addressing the existing challenges of rural electrification. The full potential of the 2S-CPV system can be harnessed by scaling up the dish to achieve power in the order of GW scale.

Declaration of Competing Interest

The authors hereby declare that there is no conflict of interest regarding publication of this paper.

Acknowledgment

The financial support provided by the Department of Science and Technology (DST), Government of India through the research project No. DST/SEED/INDO-UK/002/2011 is duly acknowledged.

References

Ajit, P.T., 2009. Solar Radiant Energy over India. India Meteorological Department, Ministry Of Earth Sciences, New Delhi.
Ancona, M.A., Bianchi, M., Diolaiti, E., Giannuzzi, A., Marano, B., Melino, F., Peretto, A., 2017. A novel solar concentrator system for combined heat and power application in residential sector. Appl. Energy 185, 1199–1209.
Asaf, B.O., Joseph, A., 2013. Estimation of multi-junction solar cell parameters. Prog. Photovolt. Res. Appl. 21, 713–723.
Assaf, B.O., Appelbaum, J., 2013. Performance analysis of concentrator photovoltaic dense-arrays under non-uniform irradiance. Sol. Energy Mater. Sol. Cells 117, 110–119.
Azur Space Solar Power GmbH, Germany, 2014. CPV triple-junction solar cell assembly – Type 3C42A data sheet, http://azurspace.com/images/products/DB_3987-00-00_3C42_AzurDesign_EFA_10x10_2014-03-27.pdf; [accessed 08.08.17].
Bunthof, L.A.A., Bos-Coenraad, J., Corbeek, W.H.M., Vlieg, E., Schermer, J.J., 2017. The illumination angle dependency of CPV solar cell electrical Performance. Sol. Energy 144, 166–174.
Chong, K.K., Yew, T.K., Wong, C.W., Tan, M.H., Tan, W.C., Lim, B.H., 2017. Dense-array concentrator photovoltaic prototype using non-imaging dish concentrator and an array of cross compound parabolic concentrators. Appl. Energy 15, 898–911.
Duffi, J.A., Beckman, W.A., 2013. Solar Engineering of Thermal Processes, fourth ed. John Wiley & Sons Inc., America.
Feuermann, D., Gordon, J.M., 2001. High-concentration photovoltaic designs based on miniature parabolic dishes. Sol. Energy 70, 423–430.
Grossman, J.W., Houser, R.M., Erdman, W.W., 1991. Prototype dish testing and analysis at Sandia national laboratories. SAN D91–1283C.
Gunther, M., Shahbazfar, R., 2011. Advanced CSP teaching materials, Chapter 7 "Solar dish technology", Deutsches Zentrum, enerMENA and DLR. enerMENA Implementation Workshop- Amman, November 3rd.
Helwa, N.H., Bahgat, A.B.G., Shafee, A.M.R., Shenawy, E.T., 2000. Maximum collectable solar energy by different solar tracking systems. Energy Sources 22 (1), 23–34.
Herrero, R., Victoria, M., Askins, S., Domínguez, C., Antón, I., Sala, G., Berrios, J., 2010. Indoor characterization of multi-junction solar cells under non-uniform light patterns. AIP Conf. Proc. 1277, 36–38.
Jaffe, L.D., 1982. Optimization of dish solar collectors with and without secondary concentrators. JPL Technical U.S. Department of Energy. Report No. DOE/JPL-1060-.
Jafrancesco, D., Sansoni, P., Francini, F., Contento, G., Cancro, C., Privato, C., Graditi, G., Ferruzzi, D., Mercatelli, L., Sani, E., Fontani, D., 2014. Mirrors array for a solar furnace: optical analysis and simulation results. Renewable Energy 63, 263–271.
Johnston, G., Lovegrove, Luzzi, A., 2003. Optical performance of spherical reflecting elements for use with paraboloidal dish concentrators. Sol. Energy 74, 133–140.
Joseph, J.O., 2008. Non-imaging Optics in Solar Energy (Synthesis Lectures on Energy and the Environment: Technology, Science, and Society). Morgan & Claypool Publishers.
Kreske, K., 2002. Optical design of a solar flux homogenizer for concentrator photovoltaics. Appl. Opt. 41, 2053–2058.
Kumar, A., Gomathinayagam, S., Giridhar, G., Mitra, I., Vashistha, R., Meyer, R., Schwandt, M., Chhatbar, K., 2013. Field experiences with the operation of solar radiation resource assessment stations in. SolarPACES, India.
Kumar, R., Rosen, M.A., 2011. A critical review of photovoltaic-thermal solar collectors for air heating. Appl. Energy 88, 3603–3614.
Kurtz, S.R., 1996. Estimating and controlling chromatic aberration losses for two-terminal devices in refractive concentrator systems. In: 26th IEEE PVSC, pp. 361–364.
Lokeswaran, S., Mallick, T.K., Reddy, K.S., 2015. Optical analysis of secondary concentrator with homogenizer for dispersed 12 X 12 array CPV receiver. In: 11th International Conference on Concentrator Photovoltaics (CPV-11), Aix-les-Bains, France.
Lovegrove, K., Burgess, G., McCready, D., Pye, J., 2009. ANU's new 500m2 paraboloidal dish solar concentrator, LSAA Conference.
Luque, A., Hedgedus, S., 2006. Handbook of Photovoltaic Science and Engineering, second ed. John Wiley & Sons, pp. 449–450.
Mallick, T.K., Sarmah, N., Banerjee, S., Micheli, L., Reddy, K.S., Ghosh, P., Walker, G., Choudhury, S., Pourkashanian, M., Hamilton, J., Giddings, D., Walker, M., Manickam, K., Hazara, A., Balachandran, S., Lokeswaran, S., Grant, D., Nimmo, W., Mathew, A., 2013. Design concept and configuration of a hybrid renewable energy system for rural electrification in India through BioCPV project. In: International Conference on Advances in Energy Research (ICAER), Mumbai.
Meller, Y., Kribus, A., 2013. Kaleidoscope homogenizers sensitivity to shading. Sol. Energy 88, 204–214.
Meyen, S., Lüpfert, E., Pernpeintner, J., Fend, T., 2009. Optical Characterization of Reflector Material for Concentrating Solar Power Technology. Solar Paces Conference.
Micheli, L., Sarmah, N., Reddy, K.S., Luo, X., Mallick, T.K., 2015. Design, development and analysis of a densely packed 500x concentrating photovoltaic cell assembly on insulated metal substrate. Int. J. Photoenergy. 2015, 1–18.
Nishioka, K., 2006. Evaluation of InGaP/InGaAs/Ge triple-junction solar cell and optimization of solar cell's structure focusing on series resistance for high-efficiency concentrator photovoltaic systems. Sol. Energy Mater. Sol. Cells. 90, 1308–1321.
Otanicar, T.P., Theisen, S., Norman, T., Tyagi, H., Taylor, R.A., 2015. Envisioning advanced solar electricity generation: Parametric studies of CPV/T systems with spectral filtering and high-temperature PV. Appl. Energy 140, 224–233.
Rabl, A., 1976. Comparision of solar concentrators. Sol. Energy 18, 93–111.
Rabl, A., 1985. Active Solar Collectors and Their Applications. Oxford University Press.
Raed, S., Paredes, A., Cotal, H., Hayden, H., 2002. A 2-kW concentrating PV array using triple junction cells. In: Photovoltaic Specialists Conference, New Orleans, USA.
Reis, F., Pravettoni, M., Wemans, J., Sorasio, G., Brito, M.C., 2015. Modeling the effects of inhomogeneous irradiation and temperature profiles on CPV cells behavior. IEEE J. Photovoltaics 5 (1), 112–122.
Segev, G., Mittelman, G., Kribus, A., 2012. Equivalent circuit models for triple-junction concentrator solar cells. Sol. Energy Mater. Sol. Cells 98, 57–65.
Shanks, K., Sarmah, N., Rodriguez, J.P.F., Senthilarasu, S., Reddy, K.S., Fernandez, E.F., Mallick, T.K., 2016. Theoretical investigation considering manufacturing errors of a high concentrating photovoltaic of Cassegrain design and its experimental validation. Sol. Energy 131, 235–245.
Siaw, F.L., Chong, K.K., Wong, C.W., 2014. A comprehensive study of dense-array concentrator photovoltaic system using non-imaging planar concentrator. Renewable Energy 62, 542–555.

Stine, W.B., Harrigan, R.W., 1985. Solar Energy Fundamentals and Design: With Computer Applications. John Wiley & Sons.
Stolte, W.J., 1992. Engineering and Economic Evaluation of Central-Station Photovoltaic Power Plants. Electric Power Research Institute, Palo Alto, CA: TR-101255.
Tan, M.H., Chong, K.K., Wong, C.W., 2014. Optical characterization of non-imaging dish concentrator for the application of dense-array concentrator photovoltaic system. Appl. Opt. 53, 475–486.
Victoria, M., Domínguez, C., Antón, I., Sala, G., 2009. Comparative analysis of different secondary optical elements for aspheric primary lenses. Opt. Express 17, 6487–6492.
Wang, J., Yang, S., Jiang, C., Yan, Q., Lund, P.D., 2017. A novel 2-stage dish concentrator with improved optical performance for concentrating solar power plants. Renewable Energy 108, 92–97.
Xu, N., Ji, J., Sun, W., Huang, W., Li, J., Jin, Z., 2016. Numerical simulation and experimental validation of a high concentration photovoltaic/thermal module based on point-focus Fresnel lens. Appl. Energy 168, 269–281.
Yew, T.K., Chong, K.K., Lim, B.H., 2015. Performance study of crossed compound parabolic concentrator as secondary optics in non-imaging dish concentrator for the application of dense-array concentrator photovoltaic system. Sol. Energy 120, 296–309.